

# MPC-Based Human-Accompanying Control Strategy for Improving the Motion Coordination between the Target Person and the Robot

Jianwei Peng<sup>1,2</sup>, Zhelin Liao<sup>1</sup>, Hanchen Yao<sup>1,2</sup>, Zefan Su<sup>1</sup>, Yadan Zeng<sup>3</sup>, Houde Dai<sup>1,2</sup>, Senior Member, IEEE

**Abstract**—Social robots have gained widespread attention for their potential to assist people in diverse domains, such as living assistance and logistics transportation. Human-accompanying, i.e., walking side-by-side with a person, is an expected and essential capability for social robots. However, due to the complexity of motion coordination between the target person and the mobile robot, the accompanying action is still unstable. In this study, we propose a human-accompanying control strategy to improve the motion coordination for better practicability of the human-accompanying robot. Our approach allows the robot to adapt to the motion variations of the target person and avoid obstacles while accompanying them. First, a human-robot interaction model based on the separation-bearing-orientation scheme is developed to ascertain the relative position and orientation between the robot and the target person. Then, a human-accompanying controller based on behavioral dynamics and model predictive control (MPC) is designed to avoid obstacles and simultaneously track the direction and velocity of the target person. Experimental results indicate that the proposed method can effectively achieve side-by-side accompanying by simultaneously controlling the relative position, direction, and velocity between the target person and robot.

## I. INTRODUCTION

Social robots for human-robot collaboration are widely employed in diverse domains, such as companionship [1], transportation [2], medical care [3], and geriatric care [4]. Accompanying a person side by side is an essential capability for robots in these applications, as it provides a more natural and comfortable mode for human-robot interaction [5], as shown in Fig. 1.

How can the robot accompany a person side by side? Generally, accompanying a person side by side involves controlling the relative position of the robot to the target person, i.e., achieving a position of 90° toward the person and maintaining a safe distance while avoiding obstacles [6]. Some advanced human-accompanying control methods [7]–[11] have accomplished these tasks with satisfactory performance. However, these methods could not steadily and accurately coordinate the motion and actions between the target person and the robot, which is crucial for achieving

\*This work was supported in part by the Central Government Guides Local Special Funds for Science and Technology Development under Grant 2020L3028, 2021L3047. Corresponding authors: Houde Dai and Yadan Zeng.

<sup>1</sup>All authors are with the Fujian Institute of Research on The Structure of Matter, Chinese Academy of Sciences, Fuzhou 350002, China. Email: pengjianwei20@mails.ucas.ac.cn, 3211239023@fafu.edu.cn, yaohanchen21@mails.ucas.ac.cn, 228527150@fzu.edu.cn, dhd@fjirsm.ac.cn.

<sup>2</sup>Jianwei Peng, Hanchen Yao, and Houde Dai are with Fujian College, University of Chinese Academy of Sciences, Jinjiang 362216, China.

<sup>3</sup>Yadan Zeng is with the Robotics Research Centre of the School of Mechanical and Aerospace Engineering, Nanyang Technological University, Singapore. Email: yadan001@e.ntu.edu.sg.



Fig. 1. Some side-by-side accompanying applications. (a) Our robot accompanies the person shopping. (b) Unitree Go1 [1] accompanies the person running. (c) Wheelchair robot [3] for nursing care.

true accompanying behavior. Motion coordination in human-accompanying behavior refers to the robot's ability to track the direction and velocity of the target person to sustain the stability of the side-by-side formation [12]. Moreover, the direction and velocity of humans during walking are irregular, especially in dynamic environments. Thus, the robot is required to adapt to the variations in the direction and velocity of the target person, which leads to the side-by-side accompanying being more challenging to control than the following from behind [9].

In this study, we aim to design a side-by-side accompanying control strategy to improve the motion coordination between the robot and the target person while accurately controlling the relative position and direction between them. Our approach allows the robot to adapt to variations in the direction and velocity of the target person, enhancing the stability and practicability of human-accompanying robots.

## A. Related Work

Most studies focused on human-following control, i.e., following the person from behind, with impressive results, e.g., PID [13], fuzzy control [14], impedance control [15], and reinforcement learning [16]. However, only a few studies focused on the side-by-side accompanying, whereas there was limited accompanying performance [17]. Therefore, a reliable side-by-side accompanying control strategy remains to be investigated. To this end, Morioka et al. [18] proposed the virtual spring model to absorb the kinematic difference between the human and the robot, but its convergence cannot be guaranteed. Yao et al. [10] designed a PD controller to accompany the person side-by-side to expand the robot's field of view and avoid the target being obscured by walls. However, this approach cannot adapt to the velocity variations of the target person. Xue et al. [19] proposed a human-accompanying control strategy based on a virtual tracking target, which essentially converts side-by-side accompanying into following from behind. However, the control accuracy

of this approach is unexceptional. Besides, these methods ignore obstacle avoidance and the physical constraints of the robot, which pose a potential security risk to the robot.

Furthermore, integrating side-by-side accompanying into the navigation framework is a common strategy. Morales et al. [6], [20] constructed a utility-based human-accompanying model by analyzing the characteristics of two people walking side-by-side. Ferrer et al. [21] proposed a social force model-based human-awareness navigation framework, expanded by Repiso et al. [9], [22] to accompany groups of people. However, these methods have a common problem of cumbersome parameter rectification and could be tricky to migrate on different robots.

To address these shortcomings, model predictive control (MPC) is a preferred method due to its inherent advantages, such as the ability to predict future states and output optimal control actions, handle explicit constraints, and its excellent robustness. Edmonds et al. [23] and Ashe et al. [24] adopted MPC to track the path taken by the target person and maintain a safe distance from the person. However, this method only applies to following from behind, as following from a different angle requires the robot to move on a different path than the human. Yan et al. [8] utilized MPC to track a trajectory that maintains a lateral distance from the patient's predicted trajectory without considering obstacle avoidance. Sekiguchi et al. [11] proposed an uncertainty-aware companion robot controller based on nonlinear MPC and probabilistic movement primitives to achieve natural human-accompanying. However, this approach assumes that the target person's velocity is constant, yielding limited practicality. Therefore, in this study, we propose an MPC-based control strategy to control the relative position between the target person and the robot while tracking the direction and velocity of the target person.

In addition, obstacle avoidance in the human-accompanying task is unavoidable. However, it has been ignored in many previous studies (e.g., [8], [10], [11], [18], [19]). Moreover, some previous studies have noted obstacle avoidance [23], [24] but ignored the robots' naturalness in human-robot interaction (HRI). Fortunately, research on HRI indicates that robots' naturalness could be improved by mimicking human behavior [25]. As such, the behavioral dynamic [26] is preferred, which enables robot avoidance of obstacles by mimicking human walk behavior.

## B. Contributions

The main contributions are listed as:

- 1) A human-robot interaction model is developed based on the separation-bearing-orientation scheme to ascertain the relative position and orientation between the robot and the target person.
- 2) A human-accompanying controller based on MPC is designed to simultaneously control the relative position, direction, and velocity between the target person and the robot.
- 3) Behavioral dynamics are integrated into the controller as an obstacle avoidance component, enabling the

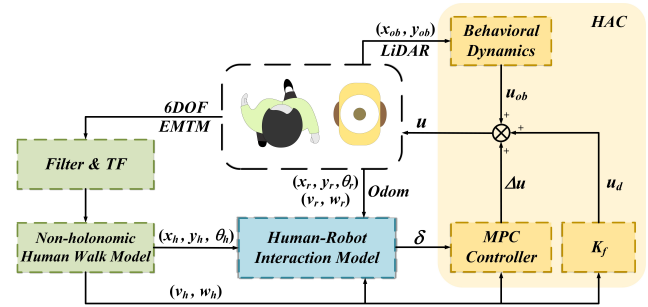


Fig. 2. Overview of the proposed scheme for the human-accompanying robot. The human-accompanying controller (HAC) is a feedforward-feedback. Behavioral dynamics are adopted for obstacle avoidance. An electromagnetic tracking module (EMTM) directly acquires the position and orientation of the target person. TF: the transformation of coordinates.

robot to mimic human obstacle avoidance behavior to improve the robot's naturalness.

## II. SYSTEM OVERVIEW

Our human-accompanying scheme, as shown in Fig. 2, mainly consists of a human-robot interaction model, a human-accompanying controller (HAC), and a wireless electromagnetic tracking module (EMTM). The EMTM<sup>1</sup> receiver is worn on the target person to receive the electromagnetic field from the transmitter mounted on the robot. Then, the high-precision position and orientation between the transmitter and receivers, i.e., the target person and the robot, can be directly acquired by the unique Amfitech<sup>1</sup> embedded algorithms. Subsequently, the high-frequency noises are filtered out using a moving average filter, and the position and orientation of the target person are converted to the global coordinate system. Next, the non-holonomic human walk model can calculate the target person's velocity, and the human-robot interaction model can ascertain the kinematic states of the human-accompanying system. Additionally, LiDAR is utilized to detect obstacles. Afterward, the HAC based on behavioral dynamics and MPC is adopted to produce control commands for the robot. Finally, these commands are then executed by the robot to drive it to accompany the target person while avoiding obstacles. The system operates in a closed loop, with perception and control updates at 30 Hz.

## III. HUMAN-ROBOT INTERACTION MODEL

In this section, we formalize the relative position and orientation relationship between the robot and the target person. Then, the kinematic states of the human-accompanying system are ascertained for the design of the human-accompanying controller.

### A. Non-holonomic Human Walk Model

We denote the target person's state as  $[x_h, y_h, \theta_h, v_h, w_h]^T$ :

$$\begin{cases} \dot{x}_h = \frac{x_h(t+\tau) - x_h(t-\tau)}{2\tau}, \dot{y}_h = \frac{y_h(t+\tau) - y_h(t-\tau)}{2\tau} \\ \dot{\theta}_h = \tan^{-1}(\dot{y}_h / \dot{x}_h) \\ \dot{v}_h = \sqrt{\dot{x}_h^2 + \dot{y}_h^2}, \dot{w}_h = \frac{\theta_h(t+\tau) - \theta_h(t-\tau)}{2\tau} \end{cases}, \quad (1)$$

<sup>1</sup> Amfitech. <https://www.amfitech.dk/>

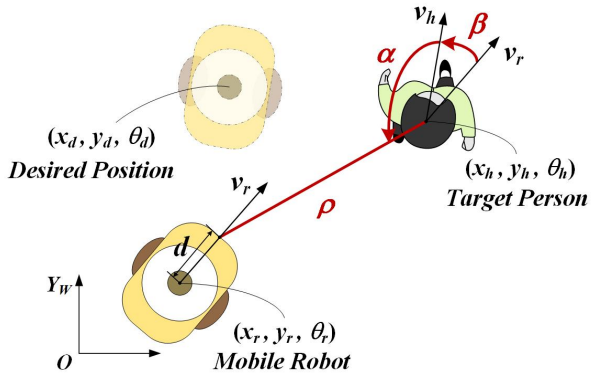


Fig. 3. Schematic of human-robot interaction model.  $\rho$  is the distance between the robot and the target person,  $\alpha$  is formed by the red connection line and the human orientation, and the relative orientation is  $\beta = \theta_h - \theta_r$ .

where  $(x_h, y_h)$  and  $\theta_h$  are the target person's position and orientation, respectively.  $v_h$  and  $w_h$  represent the forward and turning velocities of the target person, respectively.  $\tau$  is the sample period.

In the normal human walking pattern, the person moves strictly forward without lateral and longitudinal sliding, which leads to a non-holonomic model [27]. Thus the person is subject to the non-holonomic constraint:  $\dot{y}_h \cos \theta_h - \dot{x}_h \sin \theta_h = 0$ . Therefore, the target person's walk model can be given by

$$\dot{x}_h = v_h \cos \theta_h, \quad \dot{y}_h = v_h \sin \theta_h, \quad \dot{\theta}_h = w_h. \quad (2)$$

#### B. Interaction Model

The kinematics of the robot is denoted as  $\dot{x}_r = v_r \cos \theta_r, \dot{y}_r = v_r \sin \theta_r, \dot{\theta}_r = w_r$ , where  $(x_r, y_r)$  and  $\theta_r$  are the robot's position and orientation, respectively.  $v_r$  and  $w_r$  are the linear and angular velocities, respectively. The control input is  $u \in \{u \mid |v_r| \leq v_r^m, |w_r| \leq w_r^m\}$ , where  $v_r^m$  and  $w_r^m$  are the limits of linear and angular speed, respectively.

The schematic of the human-robot interaction model is given in Fig. 3, which shows that the robot accompanies the target person with a separation  $\rho$ , a relative bearing  $\alpha$ , and a relative orientation  $\beta$ . Therefore, we define the state of the human-accompanying system as  $\zeta := [\rho, \alpha, \beta]^T$ . Then we can obtain the human-robot interaction model,

$$\dot{\zeta} = \begin{bmatrix} \dot{\rho} \\ \dot{\alpha} \\ \dot{\beta} \end{bmatrix} = \begin{bmatrix} v_r \cos \gamma - v_h \cos \alpha + d w_r \sin \gamma \\ \frac{1}{\rho} (v_h \sin \alpha - v_r \sin \gamma + d w_r \cos \gamma) - w_h \\ w_h - w_r \end{bmatrix}, \quad (3)$$

where  $\gamma := \alpha + \beta$ ,  $d$  represents the distance between the mass of the center and the robot's front, and the kinematics of the target person can be obtained by (2). Moreover, the robot's position relative to the target person can be adjusted by controlling the  $\alpha$ , which equals  $\pi/2$  or  $3\pi/2$  if the robot accompanies the human on the side. If  $\beta$  converges to zeros, the robot tracks the direction of the target person.

Linearizing (3) with the Taylor series and then performing forward differencing yields the linear discrete model

$$\tilde{\zeta}(k+1) = \tilde{A}\tilde{\zeta}(k) + \tilde{B}\tilde{u}(k), \quad (4)$$

where  $\tilde{\zeta} := \zeta - \zeta_d = [\rho - \rho_d, \alpha - \alpha_d, \beta - \beta_d]^T$  is the error with respect to the desired states and  $\tilde{u} := u - u_d = [v - v_d, w - w_d]^T$  is its associated perturbation control input,

$$\tilde{A} = \begin{bmatrix} 1 & a_{12} & a_{13} \\ a_{21} & a_{22} & a_{23} \\ 0 & 0 & 1 \end{bmatrix}, \quad \tilde{B} = \begin{bmatrix} \tau \cos \gamma & \tau d \sin \gamma \\ -\frac{\tau}{\rho_d} \sin \gamma & \frac{\tau}{\rho_d} d \cos \gamma \\ 0 & -\tau \end{bmatrix},$$

$$a_{12} = \tau(-v_d \sin \gamma + v_h \sin \alpha_d + d w_d \cos \gamma),$$

$$a_{13} = -\tau(-v_d \sin \gamma + d w_d \cos \gamma),$$

$$a_{21} = -\frac{\tau}{\rho_d^2} (v_h \sin \alpha_d - v_d \sin \gamma + d w_d \cos \gamma),$$

$$a_{22} = \frac{\tau}{\rho_d} (v_h \cos \alpha_d - v_d \cos \gamma - d w_d \sin \gamma) + 1,$$

$$a_{23} = -\frac{\tau}{\rho_d} (v_d \cos \gamma + d w_d \sin \gamma).$$

## IV. HUMAN-ACCOMPANYING CONTROL STRATEGY

#### A. Control Scheme

The task of accompanying human control is mainly to control the relative position of the robot and the target person while the robot should be able to track the direction and velocity of the target person, i.e.,  $\lim_{t \rightarrow \infty} |\zeta - \zeta_d| = 0, \lim_{t \rightarrow \infty} |u - u_d| = 0$ .

Therefore, the human-accompanying control law can be designed using the perturbation control input  $\tilde{u} = u - u_d$  in the following manner

$$u(k) = u_d(k) + \tilde{u}(k), \quad (5)$$

where  $u_d(k)$  and  $\tilde{u}(k)$  represent the feedforward output and the feedback output, at the moment  $k$ , respectively. Feedforward output is the velocities that the robot needs to reach, which can be designed as  $u_d(k) = K_f u_h(k)$ , where  $u_h(k)$  can be obtained by (1), and  $K_f$  denotes gain.

Feedback command generation is based on the state error of the human-robot interaction system that drives the robot to move to the desired position. Moreover, the control increments of the robot are also considered in the feedback loop to ensure the smoothness and safety of the human-accompanying control. Therefore, we employ MPC to design the feedback controller.

#### B. Model Predictive Controller

The incremental state-space expression is

$$\begin{cases} \delta(k+1|k) = \tilde{A}\delta(k|k) + \tilde{B}\Delta\tilde{u}(k|k) \\ \eta(k|k) = \tilde{C}\delta(k|k) \end{cases}, \quad (6)$$

where  $\delta(k|k) := [\tilde{\zeta}(k|k), \tilde{u}(k|k)]^T \in \mathbb{R}^{(m+n) \times 1}$  is the incremental space state vector,  $\Delta\tilde{u}(k|k) := \tilde{u}(k|k) - \tilde{u}(k-1) \in \mathbb{R}^{m \times 1}$  is the control input increment,  $m$  and  $n$  represent the dimensions of the robot's state and control inputs, respectively.

$$\begin{aligned} \tilde{A} &= \begin{bmatrix} \tilde{A} & \tilde{B} \\ 0 & I \end{bmatrix} \in \mathbb{R}^{(m+n) \times (m+n)}, \quad \tilde{B} = \begin{bmatrix} \tilde{B} \\ I \end{bmatrix} \in \mathbb{R}^{(m+n) \times m}, \\ \tilde{C} &= [I \quad 0] \in \mathbb{R}^{n \times (m+n)}. \end{aligned}$$

The cost function can be designed as

$$J = \sum_{i=1}^{N_p} \|\zeta_i - \zeta_d\|_q^2 + \sum_{i=0}^{N_c-1} \|\Delta \tilde{u}_i\|_r^2 + \sigma \varepsilon^2, \quad (7)$$

where  $N_p$  and  $N_c$  are the prediction and control horizon, respectively, and  $N_p \geq N_c \geq 1$ .  $q > 0$  and  $r > 0$  are the weight matrices.  $\|\cdot\|^2$  represents two-norm. To avoid infeasibility, we introduce a slack variable  $M > \varepsilon > 0, M \in \mathbb{R}^+$ .

Considering the smoothness of the control and the requirements of the physical elements, the control incremental input constraints are introduced. The constraints on the control inputs can be described as  $u_{min} \leq u \leq u_{max}$ . The control increment constraints are defined as  $\Delta \tilde{u}_{min} \leq \Delta \tilde{u} \leq \Delta \tilde{u}_{max}$ . Therefore, we can rewrite the cost function (7) using the normal quadratic programming format, as

$$\min_{X(k)} J(k) = \frac{1}{2} X^T(k) H(k) X(k) + F^T(k) X(k), \quad (8)$$

$$\text{s.t. } u_{min} \leq u \leq u_{max}, \quad \Delta \tilde{u}_{min} \leq \Delta \tilde{u} \leq \Delta \tilde{u}_{max},$$

where  $X(k) = [\Delta U(k), \varepsilon(k)]^T$ ,  $\Delta U(k) = [\Delta \tilde{u}_k, \dots, \Delta \tilde{u}_{k+N_c-1}]^T$ ,

$$H(k) = \begin{bmatrix} 2(\Theta_k^T Q \Theta_k + R) & 0 \\ 0 & 2\sigma \end{bmatrix}, Q = \bigoplus_{i=1}^{N_p} q(i), R = \bigoplus_{i=1}^{N_c-1} r(i),$$

$$F(k) = [(2\delta^T(k) \Phi_k^T Q \Theta_k)^T, 0]^T, \Lambda_k^i = \bar{C} \bar{A}^i \bar{B}(k),$$

$$\Phi_k = \begin{bmatrix} \bar{C} \bar{A} \\ \bar{C} \bar{A}^2 \\ \vdots \\ \bar{C} \bar{A}^{N_p} \end{bmatrix}, \Theta_k = \begin{bmatrix} \Lambda_k^0 & 0 & \cdots & 0 \\ \Lambda_k^1 & \Lambda_{k+1}^0 & \cdots & 0 \\ \vdots & \vdots & \ddots & \vdots \\ \Lambda_k^{N_c-1} & \Lambda_{k+1}^{N_c-2} & \cdots & \Lambda_{k+N_c-1}^0 \\ \vdots & \vdots & \ddots & \vdots \\ \Lambda_k^{N_p-1} & \Lambda_{k+1}^{N_p-2} & \cdots & \Lambda_{k+N_c-1}^{N_p-N_c} \end{bmatrix}.$$

The solution of optimal control inputs obeys the receding horizon principle at every sampling time  $k$ :

$$\Delta \tilde{u}^*(k) = [I_{n \times n} \ 0 \ \cdots \ 0]_{1 \times N_c} \Delta \tilde{U}^*(k), \quad (9)$$

where  $n$  is the number of control input dimensions,  $I$  is the unit matrix. Then we can obtain the human-accompanying control law, as

$$u(k|k) = u_d(k|k) + \tilde{u}(k-1) + \Delta \tilde{u}^*(k). \quad (10)$$

### C. Behavioral Dynamics-based Obstacle Avoidance

Behavioral dynamics mimic human walking behavior, i.e., humans will adjust their walking direction in advance to avoid obstacles and generally will not have to adjust their forward speed [15]. Therefore, this method achieves obstacle avoidance by adjusting the angular velocity of the robot.

Assume that  $d_{ob}$  is the distance from the robot to the obstacle and  $d_s$  is the safe distance, then we have:

$$\ddot{\theta}_{ob} = \begin{cases} -k_0 \psi e^{-c_1 |\psi|} e^{-c_2 d_{ob}}, & d_{ob} \leq d_s \\ 0, & d_{ob} > d_s \end{cases}, \quad (11)$$

where  $\ddot{\theta}_{ob}$  is the angular acceleration in obstacle avoidance,  $\psi$  is the orientation angle of the obstacle relative to the robot,  $k_0 > 0$ ,  $c_1 > 0$ , and  $c_2 > 0$ .

Integrating (10) yields the obstacle avoidance component

$$u_{ob} = [0 \ w_{ob}]^T. \quad (12)$$

Thus, the effects of multiple obstacles can be superimposed. We can hence obtain the human-accompanying control law with obstacle avoidance:

$$u = u(k|k) + u_{ob}. \quad (13)$$

## V. SIMULATIONS AND EXPERIMENTS

In this section, the proposed side-by-side accompanying control strategy is validated and evaluated in simulation and physical environments with a differential-driven robot and compared with the PID-based side-by-side accompanying control strategy.

### A. Simulation Results

The simulation of the side-by-side accompanying is performed in Matlab 2021b, and the optimization problem in MPC is solved by quadprog<sup>2</sup>. At first, we utilize simple linear and circular trajectories to verify the effectiveness of the proposed method, as shown in Fig. 4. The robot can maintain a side-by-side formation with the target person while steadily tracking the direction and velocity of the target person. Moreover, the robot is able to quickly respond to abrupt changes in the target person's motion and smoothly converge back to equilibrium.

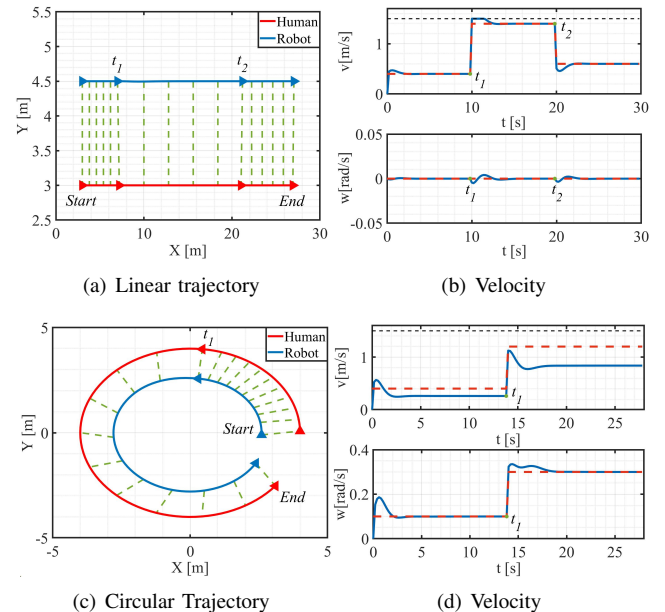


Fig. 4. Human-accompanying performance in simulations. (a) The target person moves with uniform velocity in a straight line, with the linear velocity suddenly increasing at  $t_1$  and suddenly decreasing at  $t_2$ . (c) The target person moves in a uniform circular motion, with a sudden increase in velocity by twice at  $t_1$ . The green dashed lines in (a) and (c) are the line connecting the position of the robot and the target person at a given time. (b) and (d) is the velocity curves of the robot (blue) and the target person (red), and the black dotted line is the upper boundary.

<sup>2</sup>quadprog. <https://www.mathworks.com/help/optim/ug/quadprog.html>

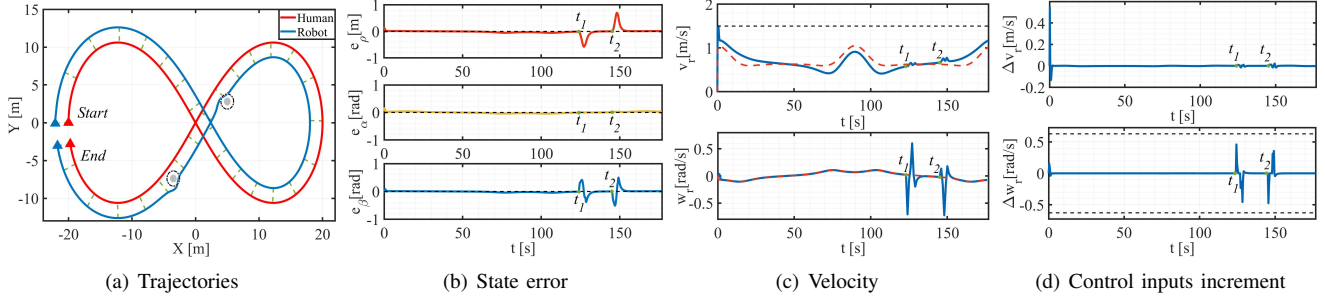


Fig. 5. Simulation for side-by-side accompanying with time-varying linear and angular velocities. At  $t_1$  and  $t_2$ , the robot bypasses the obstacle from different directions, respectively. (a) The solid gray circle is the obstacle and the black dashed circle is the safety range. (c)-(d) The red dotted lines and the blue lines are the target person's velocity and the robot's velocity, respectively. (c)-(d) The black dotted line is the upper and lower boundaries.

TABLE I  
QUANTITATIVE RESULTS OF SIMULATION WITHOUT OBSTACLES AND  
ABRUPT CHANGES IN THE PERSON'S MOTION

Trajectory	Method	RMSE			RMSV	
		$\rho$ [m]	$\alpha$ [rad]	$\beta$ [rad]	$v$ [m/s]	$w$ [rad/s]
Linear	MPC	0.00	0.02	0.00	0.08	0.00
	PID	0.14	0.30	0.00	0.19	0.00
8-shaped	MPC	0.03	0.04	0.01	0.06	0.00
	PID	0.11	0.15	0.04	0.11	0.07

Furthermore, we designed a complex 8-shaped trajectory with time-varying linear and angular velocities and set obstacles. Fig. 5(a) shows the robot's trajectory for avoiding obstacles while accompanying the target person. The robot can achieve a 90° angle toward the target person ( $\alpha$ ) and maintain a safe distance from the target person ( $\rho$ ) while tracking the direction of the target person ( $\beta$ ), as shown in Fig. 5(b). Furthermore, the robot adjusts its heading angle to avoid obstacles and can quickly reconverge to the desired state, as shown at  $t_1$  and  $t_2$ . As depicted in Fig. 5(b)-(d), despite the target person's velocity constantly changing, the robot is still able to track that velocity steadily, and the control inputs can also maintain within the predefined security bounds. On the other hand, the human-accompanying system state is almost unaffected.

Besides, we quantitatively evaluate the proposed method with a comparison to the PID-based side-by-side accompanying. The velocity of the target person in different experiments is the same without obstacles and abrupt changes in the person's motion, and the results are shown in Table I. RMSE is the root mean square error of  $[\rho, \alpha, \beta]^T$ . Meanwhile, we use the root mean square velocity (RMSV) to quantify the velocity-tracking performance of the proposed method.  $RMSV = \sqrt{\frac{1}{j} \sum_{i=1}^j (\tilde{u}_i)^2}$ , where  $j$  is the sample size of the velocity error  $\tilde{u}_i$ . Obviously, the proposed method can achieve more precise and stable relative position control and velocity tracking, and the control is more smooth. The reasons lie, on the one hand, the error of the relative position, direction, and velocity between the target person and robot are integrated into the cost function simultaneously. On the

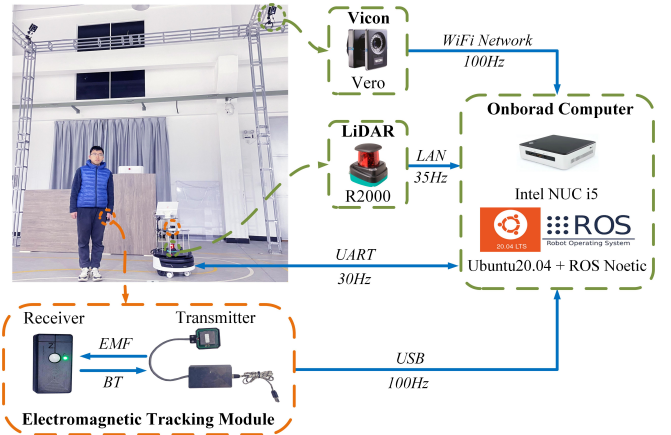


Fig. 6. Experiment setup for the human-accompanying system. EMF: electromagnetic field. BT: Bluetooth. The EMTM transmitter is mounted on the robot. The receiver is worn by the target person.

other hand, benefiting from the inherent advantages of MPC, such as the ability to predict future states and output optimal control actions and its excellent robustness. Specifically, the system in (3) is a multi-input multi-output system and the states are coupled, thus a control method such as PID cannot effectively handle the state control of that system.

### B. Real-World Experiments Results

The proposed control strategy is implemented on a differential-driven robot, which is installed with EMTM and LiDAR to acquire the target person's posture and detect obstacles, respectively, as shown in Fig. 6. The key features of EMTM versus other sensors (e.g., cameras, LiDAR, and UWB) are full six degrees of freedom tracking, high accuracy, low cost of system components, easy installation, and no line-of-sight problems [28]. Moreover, all the algorithms are integrated with the Robot Operating System (ROS, noetic) and performed online on the robot's onboard computer (Intel i5-11600 CPU). The optimization problem in MPC is solved by OSQP<sup>3</sup> with a computational rate of approximately 200Hz. The trajectory of the target person and the robot is captured by Vicon.

<sup>3</sup>OSQP. <https://osqp.org/>

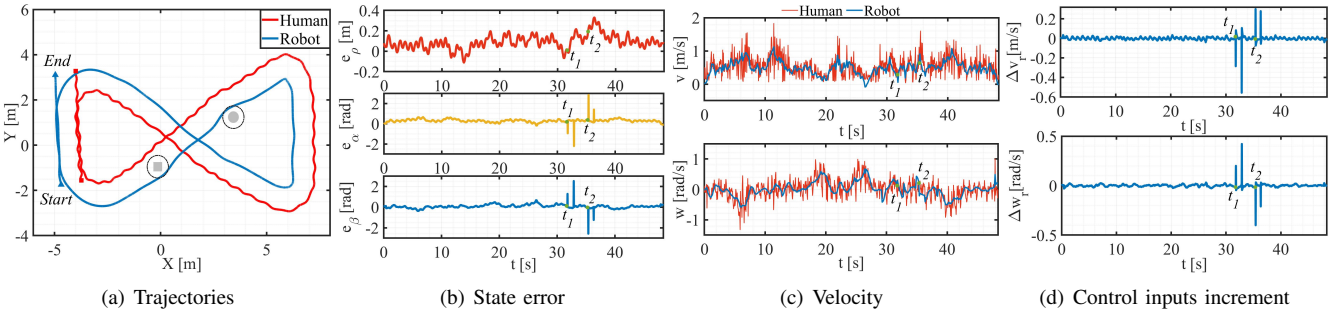


Fig. 7. Experiment for accompanying side-by-side. At  $t_1$ , the robot approaches the target person to avoid obstacles. At  $t_2$ , the robot bypasses the obstacles in a direction away from the target person. (a) The solid gray circle is the obstacle and the black dashed circle is the safety range. The red and blue lines are the target person's velocity and the robot's velocity, respectively. (d) The control input increment is the optimal solution output  $\Delta u^*$ .

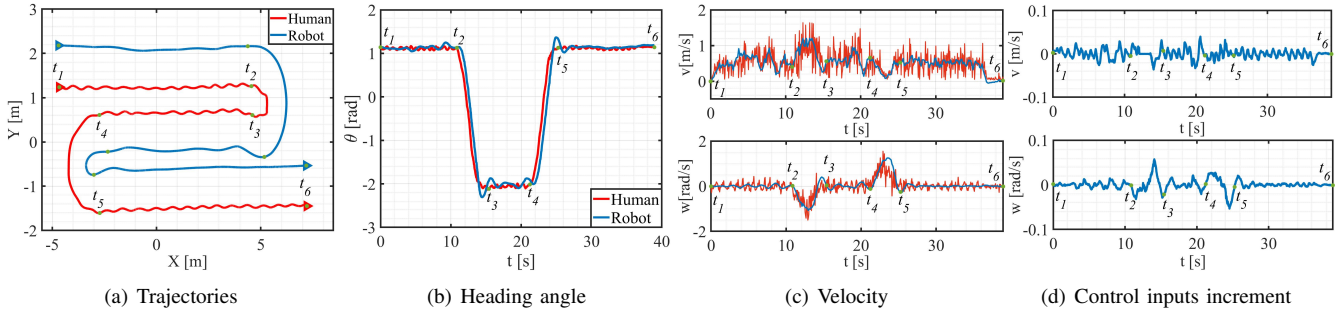


Fig. 8. Abrupt changes in the direction of the target person.  $t_1 - t_2$  and  $t_3 - t_4$ : The target person's velocity changes continuously.  $t_2 - t_3$  and  $t_4 - t_5$ : The target person's direction changes  $180^\circ$  in a short period.  $t_5 - t_6$ : The speed and direction of the target person are kept constant.

The experimental results for side-by-side accompanying are shown in Fig. 7, where the trajectory of the target person is similar to that in the simulation in Fig. 5. As shown in Fig. 7(b) and (c), the bearing angle  $\alpha$  and the relative orientation  $\beta$  are almost unaffected by variations in the velocity of the target person, and the distance between the robot and the target person  $\rho$  fluctuates within a tight range. The system state only deviates significantly when the robot avoids obstacles and can quickly reconverge to the desired state, as shown at  $t_1$  and  $t_2$ . Consequently, our method enables stable and accurate control of the relative position between the robot and the target person and effective obstacle avoidance. Furthermore, the robot can smoothly track the target person's time-varying direction and velocity, and adapt to the variation in the target person's motion, which improves the motion coordination between the target person and the robot. Notably, the experimental results support the simulation experimental results in more depth.

To further demonstrate the performance of the proposed method in tracking the direction and velocity of the target person, we designed the experiment as shown in Fig. 8. The robot responds quickly to abrupt changes in the direction of the target person with a short response time. Besides, despite significant fluctuations in the target person's velocity, the robot can steadily accompany the target person side-by-side and adapt to changes in the target person's motion. It demonstrates the proposed method's robustness and excellent performance in coordinating the motion between the target person and the robot.

## VI. CONCLUSIONS

This study presents an effective human-accompanying control strategy for improving the motion coordination between the target person and the robot. Firstly, a human-robot interaction model based on the separation-bearing-orientation scheme is built to ascertain the kinematic states of the human-accompanying system. Then, a human-accompanying controller is designed based on the MPC, which can achieve a stable and accurate relative position with the target person while adapting to changes in the target's direction and velocity. Moreover, behavioral dynamics integrated into the controller as the obstacle avoidance component allows the robot to mimic human obstacle avoidance behavior. Specifically, an EMTM is employed to acquire the target person's position and orientation directly. Experimental results show that the control strategy can drive the robot to accompany the person side by side robustly.

However, the desired state of the human-accompanying system is artificially predetermined, making this method inappropriate for the narrow passage. Thus, future work should focus on developing an adaptive decision-making strategy that considers environmental information to adjust the system state accordingly. With such advancements, the flexibility and adaptability of the human-accompanying system can be highly enhanced.

## REFERENCES

- [1] Unitree go1. [Online]. Available: <https://m.unitree.com/go1>.
- [2] Effibot. [Online]. Available: <https://www.effidence.com/en/>.

- [3] V. T. Nguyen, C. Jayawardena, and I. Ardekani, "A navigation model for side-by-side robotic wheelchairs for optimizing social comfort in crossing situations," *Robotics and Autonomous Systems*, vol. 100, pp. 27–40, 2018.
- [4] N. Savage *et al.*, "Robots rise to meet the challenge of caring for old people," *Nature*, vol. 601, no. 7893, pp. 8–10, 2022.
- [5] S. S. Honig, T. Oron-Gilad, H. Zaichyk, V. Sarne-Fleischmann, S. Olatunji, and Y. Edan, "Toward socially aware person-following robots," *IEEE Transactions on Cognitive and Developmental Systems*, vol. 10, no. 4, pp. 936–954, 2018.
- [6] L. Y. Morales Saiki, S. Satake, R. Huq, D. Glas, T. Kanda, and N. Hagita, "How do people walk side-by-side? using a computational model of human behavior for a social robot," in *Proceedings of the seventh annual ACM/IEEE international conference on Human-Robot Interaction*, 2012, pp. 301–308.
- [7] J.-S. Hu, J.-J. Wang, and D. M. Ho, "Design of sensing system and anticipative behavior for human following of mobile robots," *IEEE Transactions on Industrial Electronics*, vol. 61, no. 4, pp. 1916–1927, 2013.
- [8] S. Yan, J. Tao, J. Huang, and A. Xue, "Model predictive control for human following rehabilitation robot," in *2019 IEEE International Conference on Advanced Robotics and its Social Impacts (ARSO)*. IEEE, 2019, pp. 369–374.
- [9] E. Repiso, F. Zanlungo, T. Kanda, A. Garrell, and A. Sanfeliu, "People's v-formation and side-by-side model adapted to accompany groups of people by social robots," in *2019 IEEE/RSJ International Conference on Intelligent Robots and Systems (IROS)*. IEEE, 2019, pp. 2082–2088.
- [10] H. Yao, H. Dai, E. Zhao, P. Liu, and R. Zhao, "Laser-based side-by-side following for human-following robots," in *2021 IEEE/RSJ International Conference on Intelligent Robots and Systems (IROS)*. IEEE, 2021, pp. 2651–2656.
- [11] S. Sekiguchi, A. Yorozu, K. Kuno, M. Okada, Y. Watanabe, and M. Takahashi, "Uncertainty-aware non-linear model predictive control for human-following companion robot," in *2021 IEEE International Conference on Robotics and Automation (ICRA)*. IEEE, 2021, pp. 8316–8322.
- [12] E. Prassler, D. Bank, and B. Kluge, "Motion coordination between a human and a mobile robot," in *IEEE/RSJ International Conference on Intelligent Robots and Systems*, vol. 2. IEEE, 2002, pp. 1228–1233.
- [13] N. Yao, E. Anaya, Q. Tao, S. Cho, H. Zheng, and F. Zhang, "Monocular vision-based human following on miniature robotic blimp," in *2017 IEEE International Conference on Robotics and Automation (ICRA)*. IEEE, 2017, pp. 3244–3249.
- [14] N. Van Toan, M. Do Hoang, P. B. Khoi, and S.-Y. Yi, "The human-following strategy for mobile robots in mixed environments," *Robotics and Autonomous Systems*, vol. 160, p. 104317, 2023.
- [15] H. Tian and X. Ma, "Behavioral dynamics-based impedance control for collision avoidance of human-following robots," in *2022 IEEE International Conference on Real-time Computing and Robotics (RCAR)*. IEEE, 2022, pp. 349–354.
- [16] L. Kästner, B. Fatloun, Z. Shen, D. Gawrisch, and J. Lambrecht, "Human-following and-guiding in crowded environments using semantic deep-reinforcement-learning for mobile service robots," in *2022 International Conference on Robotics and Automation (ICRA)*. IEEE, 2022, pp. 833–839.
- [17] M. J. Islam, J. Hong, and J. Sattar, "Person-following by autonomous robots: A categorical overview," *The International Journal of Robotics Research*, vol. 38, no. 14, pp. 1581–1618, 2019.
- [18] K. Morioka, J.-H. Lee, and H. Hashimoto, "Human-following mobile robot in a distributed intelligent sensor network," *IEEE Transactions on Industrial Electronics*, vol. 51, no. 1, pp. 229–237, 2004.
- [19] G. Xue, H. Yao, Y. Zhang, J. Huang, L. Zhu, and H. Dai, "Uwb-based adaptable side-by-side following for human-following robots," in *2022 IEEE International Conference on Robotics and Biomimetics (ROBIO)*. IEEE, 2022, pp. 333–338.
- [20] R. Murakami, L. Y. Morales Saiki, S. Satake, T. Kanda, and H. Ishiguro, "Destination unknown: walking side-by-side without knowing the goal," in *Proceedings of the 2014 ACM/IEEE international conference on Human-robot interaction*, 2014, pp. 471–478.
- [21] G. Ferrer, A. Garrell, and A. Sanfeliu, "Robot companion: A social-force based approach with human awareness-navigation in crowded environments," in *2013 IEEE/RSJ International Conference on Intelligent Robots and Systems*. IEEE, 2013, pp. 1688–1694.
- [22] E. Repiso, A. Garrell, and A. Sanfeliu, "People's adaptive side-by-side model evolved to accompany groups of people by social robots," *IEEE Robotics and Automation Letters*, vol. 5, no. 2, pp. 2387–2394, 2020.
- [23] M. Edmonds, T. Yigit, V. Hong, F. Sikandar, and J. Yi, "Optimal trajectories for autonomous human-following carts with gesture-based contactless positioning suggestions," in *2021 American Control Conference (ACC)*. IEEE, 2021, pp. 3896–3901.
- [24] A. K. Ashe and K. M. Krishna, "Maneuvering intersections & occlusions using mpc-based prioritized tracking for differential drive person following robot," in *2021 IEEE 17th International Conference on Automation Science and Engineering (CASE)*. IEEE, 2021, pp. 1352–1357.
- [25] T. Kruse, A. K. Pandey, R. Alami, and A. Kirsch, "Human-aware robot navigation: A survey," *Robotics and Autonomous Systems*, vol. 61, no. 12, pp. 1726–1743, 2013.
- [26] B. R. Fajen and W. H. Warren, "Behavioral dynamics of steering, obstacle avoidance, and route selection," *Journal of Experimental Psychology: Human Perception and Performance*, vol. 29, no. 2, p. 343, 2003.
- [27] G. Arechavaleta, J.-P. Laumond, H. Hicheur, and A. Berthoz, "On the nonholonomic nature of human locomotion," *Autonomous Robots*, vol. 25, no. 1, pp. 25–35, 2008.
- [28] H. Gietler, H. Ammari, and H. Zangl, "Robust electromagnetic pose estimation for robotic applications," *IEEE Transactions on Instrumentation and Measurement*, vol. 69, no. 7, pp. 4258–4269, 2019.